UNIVERSITY OF WATERLOO - Faculty of Science

EFFECT OF LOADING RATE ON PINAWA GRANITE

Prepared by P.A. Tibble
ID 88008420

MRL 89-148

September 1, 1989

Energy, Mines and Resources Canada
Énergie, Mines et Ressources Canada

Canada Centre for Mineral and Energy Technology
Centre canadien de la technologie des minéraux et de l'énergie

CANMET

555 Booth Street
Ottawa, Canada
K1A 0G1

555 rue Booth
Ottawa, Canada
K1A 0G1

August 29, 1989

Mr. J.C. Wilson,
Director,
Co-operative Education and Career Services,
University of Waterloo,
Waterloo, Ontario,
N2L 3G1

Dear Mr. Wilson,

This report entitled 'Effects of Loading Rate on Pinawa Granite', was prepared as my 1b work term report for the Mining Research Laboratories (MRL), branch of the Canada Centre for Mineral and Energy Technology (CANMET), Energy Mines and Resources Canada. This is my first work-term report.

MRL undertakes rock mechanics studies for government agencies and the mining sector. I was supervised by Mr. R. Jackson and Mr. B Gorski. This work was done as part of a continuing research programme for Atomic Energy Canada Limited (AECL), to investigate the mechanics of long term nuclear waste disposal.

This report has been prepared and written by me and has not received any previous academic credit at this or any other institution. I would like to thank Mr. R. Jackson and Mr. B. Gorski for their assistance and support, and also Ms. G. Hunter and Mrs. J. Folta for their assistance in preparing this document.

Sincerely,

P. A. Tibble
ID 88008420

Canada

UNIVERSITY OF WATERLOO
Faculty of Science

EFFECT OF LOADING RATE ON PINAWA GRANITE

Mining Research Laboratories
Canadian Mine Technology Laboratory
Bells Corners, Ontario

prepared by

P.A.Tibble
ID 88008420
1B APPLIED EARTH SCIENCE (GEOLOGY OPTION)
1 SEPTEMBER 1989

ABSTRACT

This report investigates the effect of loading rate on the material properties and dynamic constants of granitic samples from the Underground Research Laboratory (URL), near Pinawa, Manitoba.

Atomic Energy Canada Limited (A.E.C.L.) is presently investigating the feasibility of long-term underground storage of nuclear waste using test samples from the Pinawa batholith.

It was concluded that the loading rates studied had no significant effect on the Tangent Modulus of Elasticity or Poisson's ratio. The uniaxial compressive strength of the samples, however, decreased with the loading.

It is recommended that more testing programmes be initiated and new methods for longterm effects of load, and other natural geologic occurrences be devised to better reflect the storage conditions.

TABLE OF CONTENTS

LIST OF FIGURES

LIST OF TABLES

INTRODUCTION

The storage of waste produced through nuclear fission has presented very special, and very difficult problems for industry and society. The problems arise from the extreme danger that fission products poise to the environment and the length of time required for safe disposal.

Atomic Energy of Canada Limited (A.E.C.L) is presently investigating the feasibility of storage chambers cut deep within stable rock formations. If rock formation are found that exhibit extreme stability over time of such great magnitude, a realistic solution to the storage needs of nuclear waste would be available.

This report investigates the effects of load over time on a rock mass. Since the storage of nuclear waste involves an extended time period, the effects of load on the strength of rock is very necessary. Uniaxial compression tests were performed on 21 samples of granite at three different loading rates, 0.75 megapascals per second (MPa/s), 0.075 MPa/s and 0.0075 MPa/s.

Values for uniaxial compressive strength, Young's modulus and Poisson's ratio were calculated. The effects of the reduced loading rates are discussed through interpretation of existing rock failure theories.

1.0 Geological Description of Test Samples

Test samples originated from Test Room 9 at the 240 meter level of the Underground Research Laboratory (URL) excavation in the Lac du Bonnet batholith near Pinawa, Manitoba. The samples were 45 mm in diameter with a granitic composition and a coarse grained texture. Mineralogical compositions were approximately 30% K-feldspar, 30% plagioclase, 30% or slightly less quartz and 10% or slightly more mafic minerals, with biotite dominating.

1.1 Preparation of Samples

Core samples selected for testing are first cut using a water-cooled diamond impregnated saw. They are cut to a length slightly longer then the desired final length to allow for sufficient lapping. Samples should have a final length-to-diameter ratio of 2.5:1. The samples are next lapped using a double-lapping machine until the parallelity of the ends is within 0.001 inch and they are as perpendicular to the long axis as possible. With the samples properly prepared physical measurements of length and diameter can be obtained. (Table 1.)

2.0 Determination of Ultrasonic Velocity Constants

Compressional wave and shear wave velocities as well as Dynamic Young's Modulus, Dynamic Shear Modulus, and the Dynamic Poisson's ratio are determined using ultrasonic pulse velocity measuring equipment. (Fig. 1.) The transmitter imparts a mechanical impulse to the sample and the arrival time of the wave is observed using the oscilloscope. The time required for the wave to transverse the sample's length is used to calculate the wave velocity.

$$V = \frac{l}{t}$$

Where V = dynamic Young's modulus

l = Poisson's ratio

t = shear wave velocity

The dynamic Young's Modulus, dynamic Shear Modulus, and the dynamic Poisson's ratio, referred to as the dynamic constants, are calculated from the wave velocities and the sample's density.

$$E_d = \frac{\rho V_s^2 3(V_p^2 - 4V_s^2)}{V_p^2 - V_s^2}$$

$$\nu_d = \frac{V_p^2 - 2V_s^2}{2(V_p^2 - V_s^2)}$$

Where E_d = dynamic Young's modulus

ρ_d = Poisson's ratio

V_s = shear wave velocity

V_p = compressive wave velocity

2.1 Strain Gauge Application

Surface areas selected for gauge placement are sanded and washed down with acetone to remove surface roughness, dirt, and oils and to allow for a better bonding between sample and gauge. Micro-Measurements, Inc. general purpose 500BH strain gauges, (Fig. 2) and a two component glue were used on the test samples.Two axial strain gauges are applied diametrically opposing one another and two circumferential gauges are applied in the same manner. Each pair of gauges is wired in series and the lead wires attached by solder (Fig. 3). A jacket of heat shrinkable tubing is placed over the prepared sample to protect the test personnel and test equipment, and to allow examination of failure characteristics.

3.0 Loading Tests and Data Presentation

The test samples were loaded to failure using a Material Testing System (MTS) 815 Rock Mechanics Test System operated by the senior technologist. The lead wires from the strain gauges were attached to two Bruel and Kjaer type 1526 strain indicators. The circuit was configured to form a half wheatstone bridge that uses dummy arms of the same gauge factor to compensate for effects due to temperature and lead length. Seven samples were tested at each loading rate; 0.75 megapascals per second (MPa/sec), 0.075 MPa/sec, and 0.0075 MPa/sec. Load, axial strain and circumferential strain data was recorded and later transferred to the facilities VAX computer system for analysis. Graphical interpretation was conducted, plotting stress against strain (Figs. 4-25) and tables showing the modulus of elasticity, Poisson's ratio, uniaxial compressive strength and calculated mean values were produced. (Tables 2-6)

3.1 Discussion and Interpretation

Test results from the load rate experiments indicate that the uniaxial compressive strength of the granitic samples was directly affected by the rate at which they were loaded to failure. Suggested load rates between 0.50 MPa/s and 1.00 MPa/s are used in standard laboratory experiments to determine the uniaxial compressive strength of rock samples and one of the loading rates used in this set of experiments, 0.75 MPa/s is within these parameters. When the values of the uniaxial compressive strength for this standardized loading rate are compared to the values obtained from the reduced loading rates, a dramatic decrease in the uniaxial compressive strength is observed. A notable decrease of 8.9% exists between the first loading rate of 0.75 MPa/s and the second loading rate of 0.075 Mpa/s. A further decrease of 7.3% was noted between the second loading rate and the third of .0075 Mpa/s. An over all decrease of 15.6% or 28 MPa was observed over the entire load-rate range. The Tangent modulus of elasticity was consistently within deviations that can be attributed to variances in rock composition and sample preparation. There was no evidence to indicate that the tangent modulus of elasticity was affected by different loading rates. Also of interest is the large variance of 11 standard deviations observed for the uniaxial compressive strengths of the samples that were failed at the load rate of 0.0075 MPa/s. This large field of failure strengths suggests that with increased loading time failure planes have greater opportunity to manifest themselves along existing weaknesses inherent in the rock; and secondly, that such weaknesses exist and are unique to each sample.

3.2 Theories on Rock Failure and Interpretation

Many theories address the mechanism that actually leads to failure in rock and other solid materials and the effects of strain over time on material strength and failure. The Griffith Theory of Rupture [2] was an early and quite explanation of the mechanism that causes failure in solids. Griffith based much of his theory on considerable experiments that he conducted on glass and metal solids. The Griffith Theory of rupture, stated simply, explains that failure results as micro-cracks grow in response to load. The growth occurs as the extreme tension located at the crack tip exceeds the elastic modulus for the material. These micro-cracks can be idealized as thin ellipses and as a result of their shape extreme tensions exist at their tips. Any stress acting on the sample will be greatly magnified at crack tips, and failure can result at values far lower than expected values predicted by the material's modulus of elasticity. Griffith further postulated that the multitude of existing micro-cracks in the solid may coalesce to form larger micro-cracks and micro-faults directed by the applied force. However, it is not entirely clear how curved micro-cracks might coalesce to form microscopic fractures [1]. Griffith's theories were partially revised by McClintock and Walsh to better explain rock failure. McClintock and Walsh assumed that as a load is imparted to a test sample the ellipse shaped micro-cracks close, creating frictional forces that might then develop at the contacts of crack surfaces to influence crack growth and ultimately failure [1].The samples were tested with end platens made of hardened steel with the same diameter as the test sample. The end platens create a region of uneven stress distribution that forms a cone extending at approximately 45 degrees until a point is formed within the sample [4]. The directing of a region of uneven stress combined with a loading rate slow enough to allow for crack propagation in accordance with Griffith's rupture theories and modified Griffith theories would lead to the prediction of conically shaped and diagonal failure planes. Such failure characteristics were observed in test samples from all three loading rates, with no one loading rate being dominated by cone, wedge or diagonal failure characteristics.

The movement of one crack creates a field of extremely fast moving stresses that can cause further cracks to occur. The cohesion of the sample is reduced as the cracks spread to the sample's surface, redistributing the load to smaller unbroken sections of the sample. All these factors act to reduce the strength of the sample [3]. The velocity at which the cracks grow is dependent on the physical properties of the sample. The theory of crack stress being an initiator for secondary crack formation leading to failure strongly suggests that the strength of a test sample will be a function of time. Tests conducted on glass blocks yielded results that suggest the platen restrictions do not encourage directed failure but limit the formation of a series of straight cracks connected by many jagged transverse cracks [3]. This failure characteristic was again observed in all samples from all three loading rates and is referred to as axial splitting.

While no one theory best explains observed rock failure, the cumulation of both directional crack propagation through Griffith and modified Griffith rupture theories and the development of axial splitting, as observed in both glass blocks [3] and charcoal grey granite, provide a reasonable and realistic model rock failure, as observed in the test samples from the Pinawa batholith.

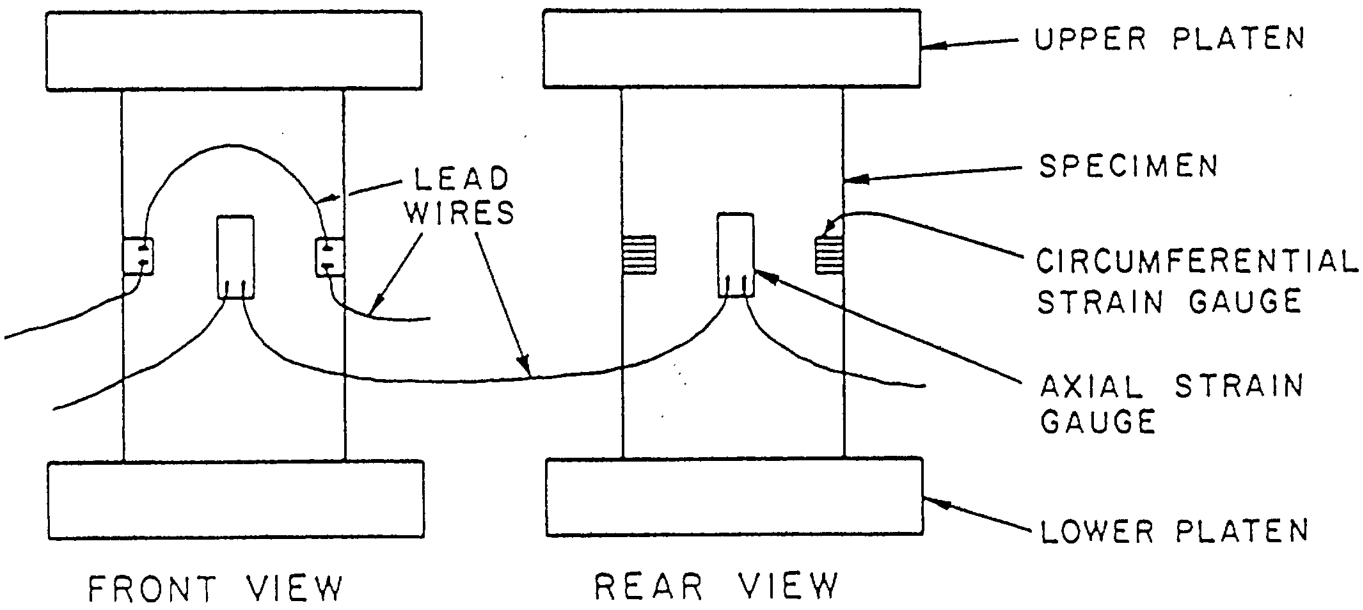

Figure 3 wiring of gauged sample.

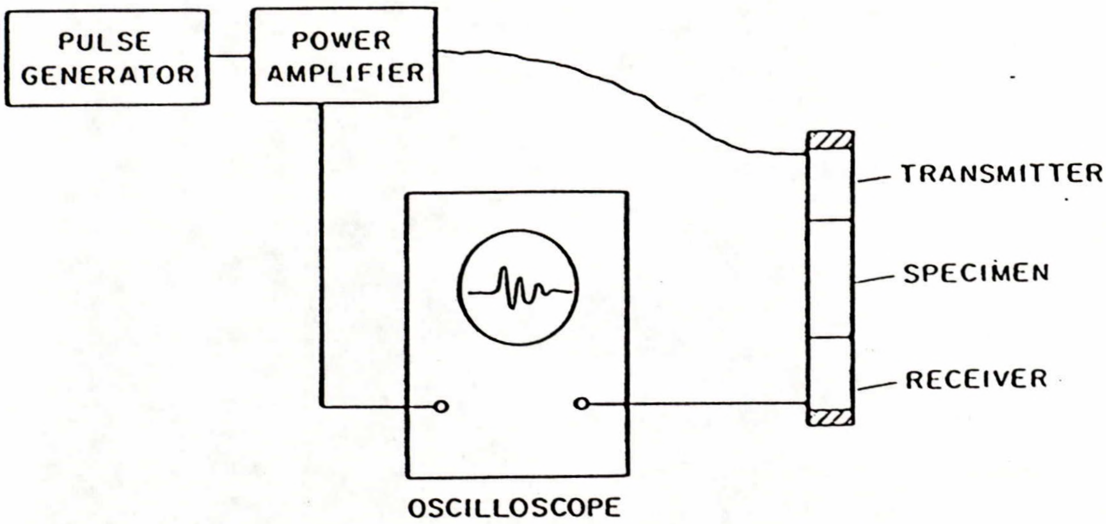

Figure 1 schematic of ultrasonic pulse measuring equipment.

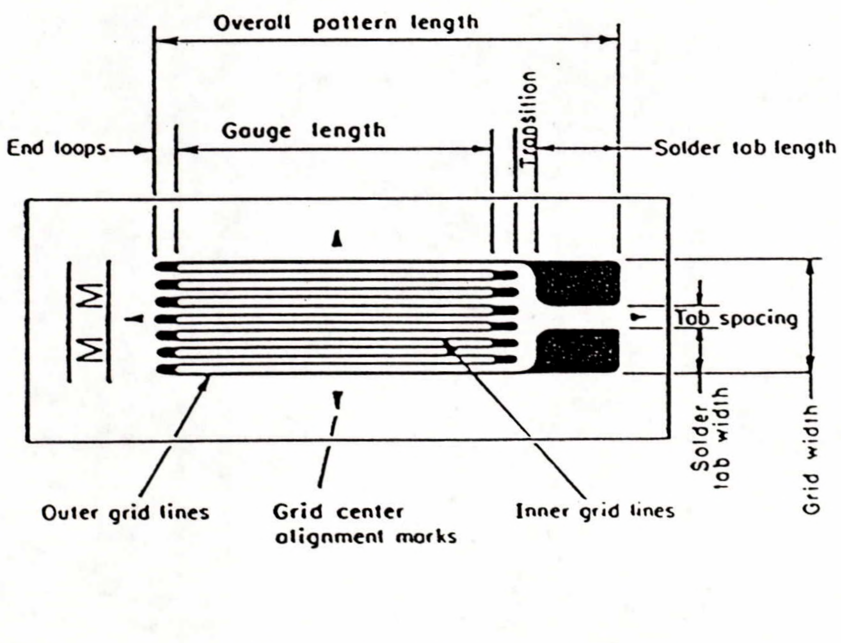

Figure 2 Micro-Measurements Inc. general purpose 500BH strain gauge.

Table 1: Summary of Specimen Dimensions and Density

Specimen Identification	Length (mm)	Diameter (mm)	Density (Mg/m^3)
209-018-EXT7 8.27	101.85	44.74	2.63
8.37	103.78	44.80	2.63
8.47	105.08	44.71	2.63
9.04	104.94	44.70	2.63
9.17	103.00	44.78	2.63
9.37	102.90	44.79	2.62
9.48	102.49	44.75	2.63
10.72	100.68	44.82	2.63
10.83	104.24	44.85	2.62
11.29	101.09	44.79	2.63
11.40	100.67	44.80	2.63
11.50	102.91	44.84	2.63
11.61	101.65	44.81	2.63
11.72	101.71	44.83	2.63
11.97	102.73	44.80	2.64
12.06	102.10	44.82	2.63
12.16	101.91	44.82	2.63
12.27	100.89	44.84	2.63
12.37	104.08	44.86	2.63
12.50	103.23	44.80	2.63
12.61	103.06	44.80	2.63

Table 2: Summary of Ultrasonic Velocity and Dynamic Properties for URL Loading Rate Specimens

Specimen Identification	P-wave Velocity (km/s)	S-wave Velocity (km/s)	Dynamic Young's Modulus (GPa)	Dynamic Shear Modulus (GPa)	Dynamic Poisson's Ratio
209-018-EXT7 8.27	4.41	3.00	50.62	23.59	0.07
8.37	4.37	2.80	47.41	20.55	0.15
8.47	4.35	2.90	48.69	22.07	0.10
9.04	4.38	2.92	49.42	22.48	0.10
9.17	4.39	2.84	48.41	21.27	0.14
9.37	4.33	2.92	48.42	22.42	0.08
9.48	4.33	2.92	48.58	22.38	0.08
10.72	4.85	3.29	61.21	28.46	0.08
10.83	4.66	3.09	55.53	25.08	0.11
11.29	4.42	2.81	48.21	20.80	0.16
11.40	4.46	2.76	47.70	20.05	0.19
11.50	4.58	2.78	49.12	20.33	0.21
11.61	4.46	3.13	52.30	25.76	0.02
11.72	4.68	3.19	57.18	26.80	0.07
11.97	4.31	3.24	47.31	27.71	-0.15
12.06	4.47	3.08	52.31	24.98	0.05
12.16	4.51	3.02	52.46	23.91	0.10
12.27	4.60	3.05	54.20	24.46	0.11
12.37	4.51	3.03	52.59	24.13	0.10
12.50	4.63	3.17	55.89	26.48	0.06
12.61	4.54	3.04	53.16	24.31	0.09
Mean	4.48 (0.14)	3.00 (0.15)	51.46 (3.75)	23.72 (2.46)	0.09 (0.07)

Table 3: Summary of Uniaxial Compression Properties: Loading Rate = 0.75 MPa/s

Specimen Identification	Uniaxial Compressive Strength (MPa)	Tangent Modulus of Elasticity (GPa)								Poisson's Ratio
		10 MPa	20 MPa	30 MPa	40 MPa	50 MPa	60 MPa	50%	75%	
209-018-EXT7 8.27	187	29.31	43.35	52.27	58.03	61.70	63.74	65.94	61.66	0.25
9.04	186	23.08	39.03	48.76	54.97	58.97	61.30	64.39	61.31	0.29
9.48	191	29.04	42.65	51.59	57.31	60.90	62.83	65.80	65.34	0.23
11.29	175	35.10	45.52	53.19	58.26	61.52	63.32	64.78	60.31	0.26
11.61	170	28.95	44.25	54.11	60.03	63.36	64.63	65.76	67.94	0.25
12.06	181	31.52	45.10	54.03	59.73	63.27	65.09	66.76	62.55	0.26
12.37	167	29.99	39.57	46.52	51.39	54.80	57.10	59.46	55.43	0.27

Table 4: Summary of Uniaxial Compression Properties: Loading Rate = 0.075 MPa/s

Specimen Identification	Uniaxial Compressive Strength (MPa)	Tangent Modulus of Elasticity (GPa)								Poisson's Ratio
		10 MPa	20 MPa	30 MPa	40 MPa	50 MPa	60 MPa	50%	75%	
209-018-EXT7 8.37	171	32.54	44.14	53.05	57.95	60.33	61.94	63.81	60.19	0.29
9.17	176	27.09	39.89	50.00	56.47	60.80	63.98	68.49	64.84	0.29
10.72	161	35.42	45.23	52.75	57.08	59.30	60.71	61.68	56.23	0.20
11.40	157	39.08	48.33	55.31	59.21	61.07	62.55	64.85	68.20	0.34
11.72	159	32.60	43.96	52.40	57.12	59.49	61.05	62.34	60.28	0.25
12.16	164	26.54	40.29	49.88	55.09	57.68	59.50	61.84	61.00	0.19
12.50	162	29.04	38.70	47.69	53.37	57.05	59.81	63.53	64.19	0.32

Table 5: Summary of Uniaxial Compression Properties: Loading Rate = 0.0075 MPa/s

Specimen Identification	Uniaxial Compressive Strength (MPa)	Tangent Modulus of Elasticity (GPa)								Poisson's Ratio
		10 MPa	20 MPa	30 MPa	40 MPa	50 MPa	60 MPa	50%	75%	
209-018-EXT7 8.47	174	32.81	44.43	52.97	57.63	59.82	61.38	63.93	63.54	0.24
9.37	153	28.37	40.54	49.36	54.82	58.23	60.72	63.34	63.43	0.27
10.83	150	34.03	46.03	54.61	59.23	61.33	62.76	64.10	63.62	0.29
11.50	147	34.82	46.83	55.57	60.89	64.02	66.00	66.99	63.96	0.27
11.97	147	34.19	45.24	54.47	60.53	64.56	67.28	68.97	67.02	0.30
12.27	156	34.10	45.50	55.61	61.17	63.86	65.48	66.55	62.05	0.32
12.61	140	27.12	39.89	49.28	55.12	58.75	61.08	62.38	59.51	0.28

Table 6: Mean Uniaxial Compression Properties for URL Loading Rate Specimens

Loading Rate (MPa/s)	Uniaxial Compressive Strength (MPa)	Tangent Modulus of Elasticity (GPa)								Poisson's Ratio
		10 MPa	20 MPa	30 MPa	40 MPa	50 MPa	60 MPa	50%	75%	
0.75	180 (9)	29.57 (3.59)	42.78 (2.57)	51.50 (2.86)	57.10 (3.02)	60.65 (2.98)	62.57 (2.71)	64.70 (2.44)	62.08 (3.94)	0.26 (0.02)
0.075	164 (7)	31.76 (4.56)	42.93 (3.44)	51.58 (2.53)	56.61 (1.91)	59.39 (1.53)	61.36 (1.58)	63.79 (2.37)	62.13 (3.91)	0.27 (0.06)
0.0075	152 (11)	32.21 (3.13)	44.07 (2.74)	53.12 (2.74)	58.48 (2.68)	61.51 (2.66)	63.53 (2.68)	65.18 (2.36)	63.30 (2.25)	0.28 (0.03)

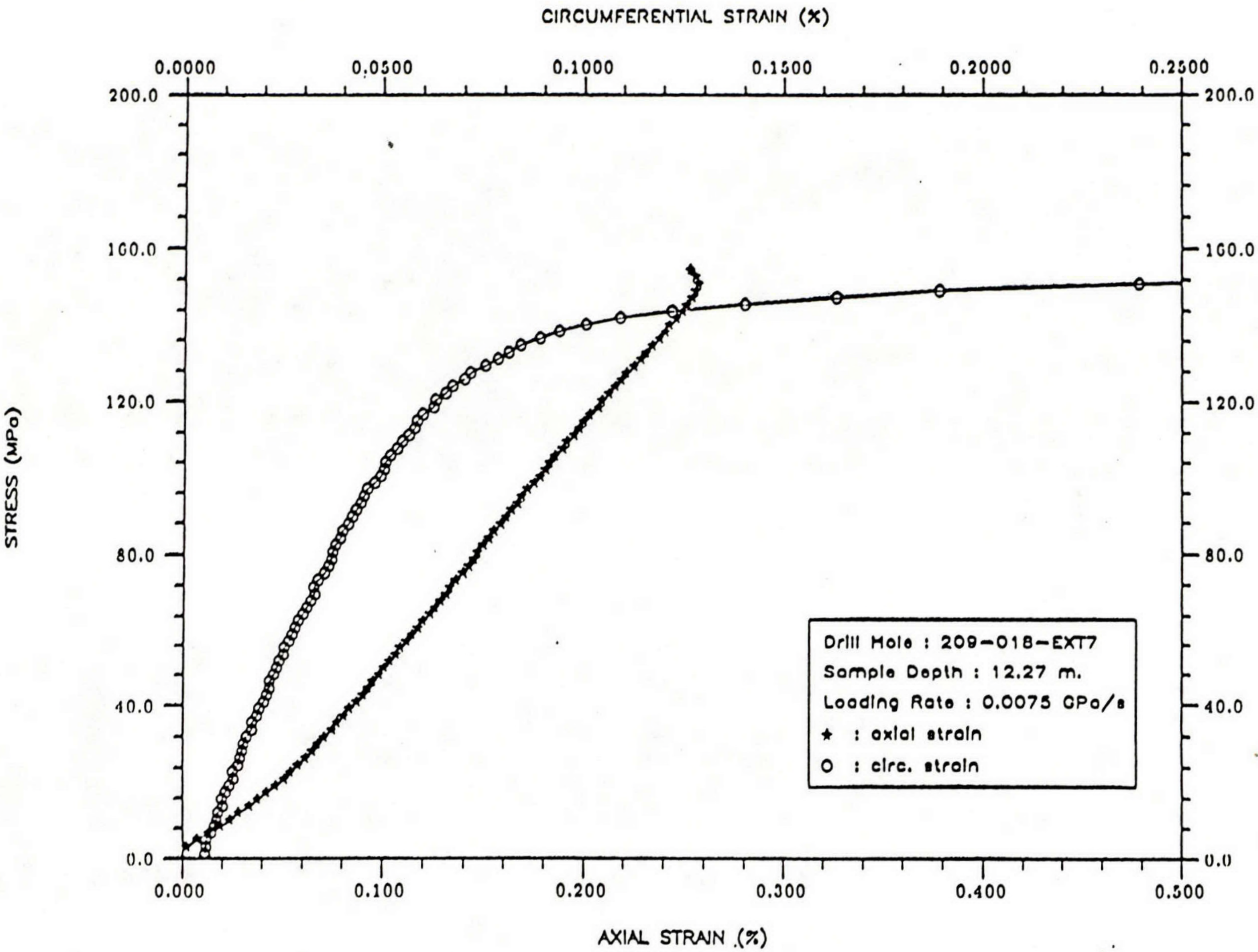

Figure 23 Axial and circumferential stress/strain curves for URL loading rate specimens

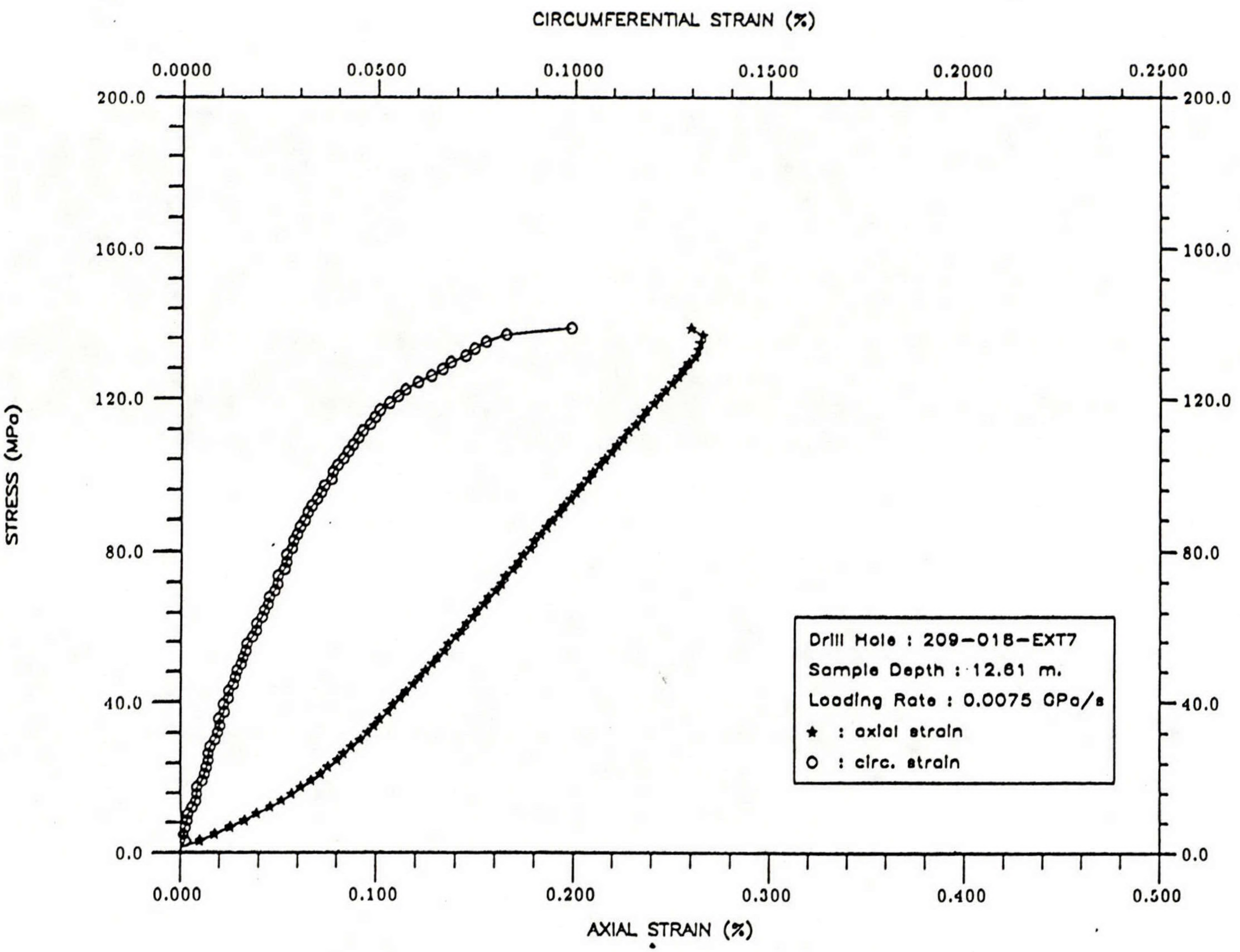

Figure 24 Axial and circumferential stress/strain curves for URL loading rate specimens

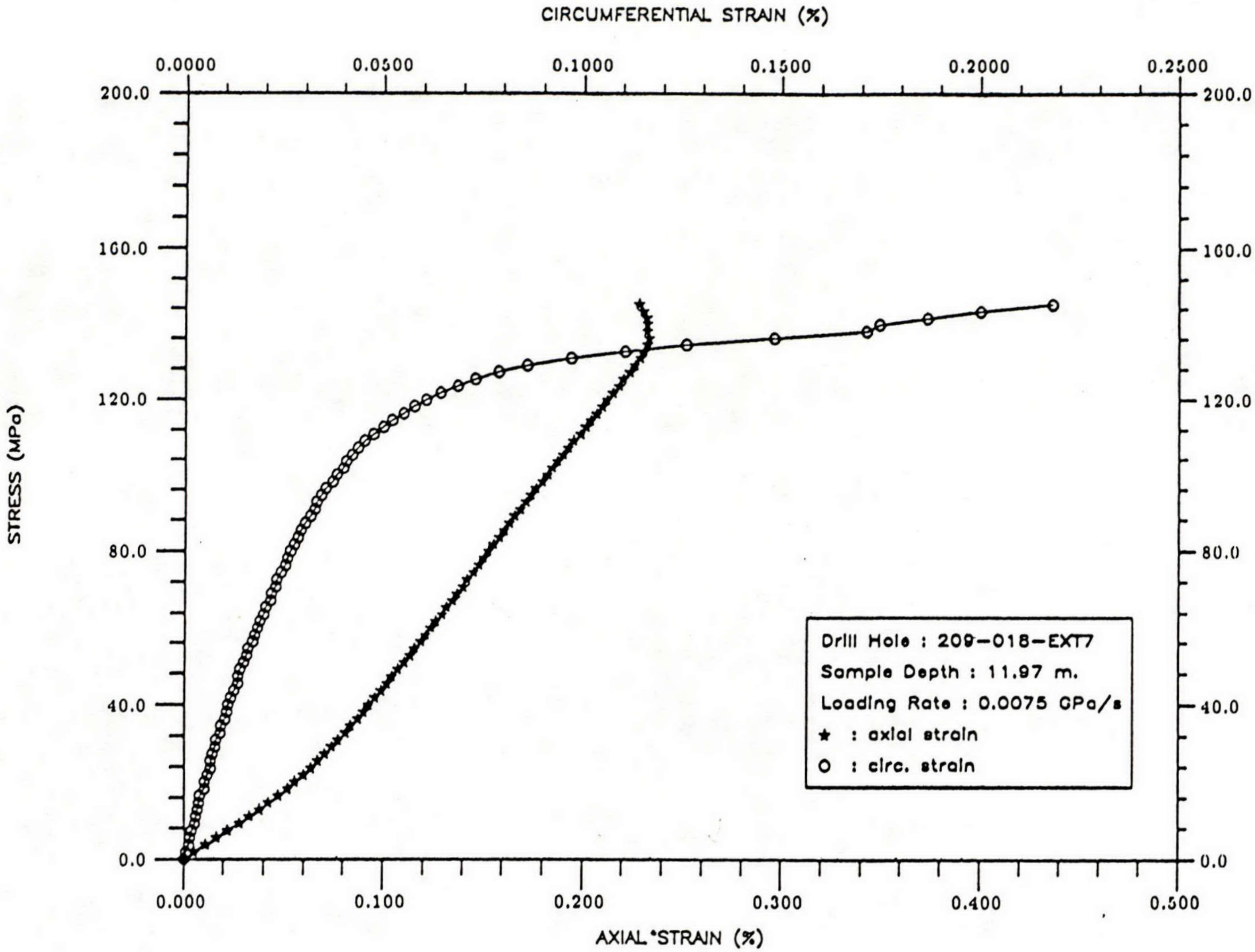

Figure 22 Axial and circumferential stress/strain curves for URL loading rate specimens

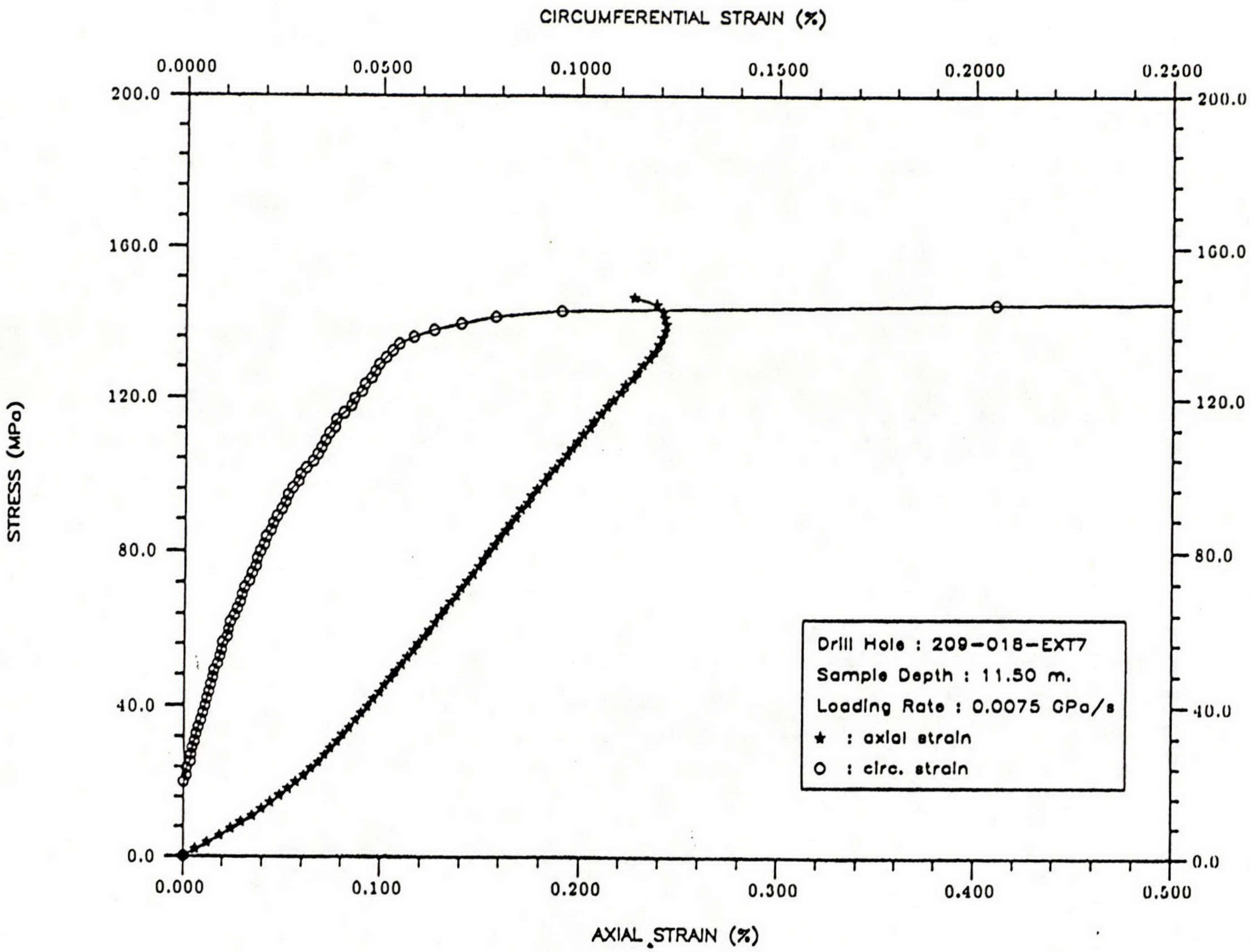

Figure 21 Axial and circumferential stress/strain curves for URL loading rate specimens

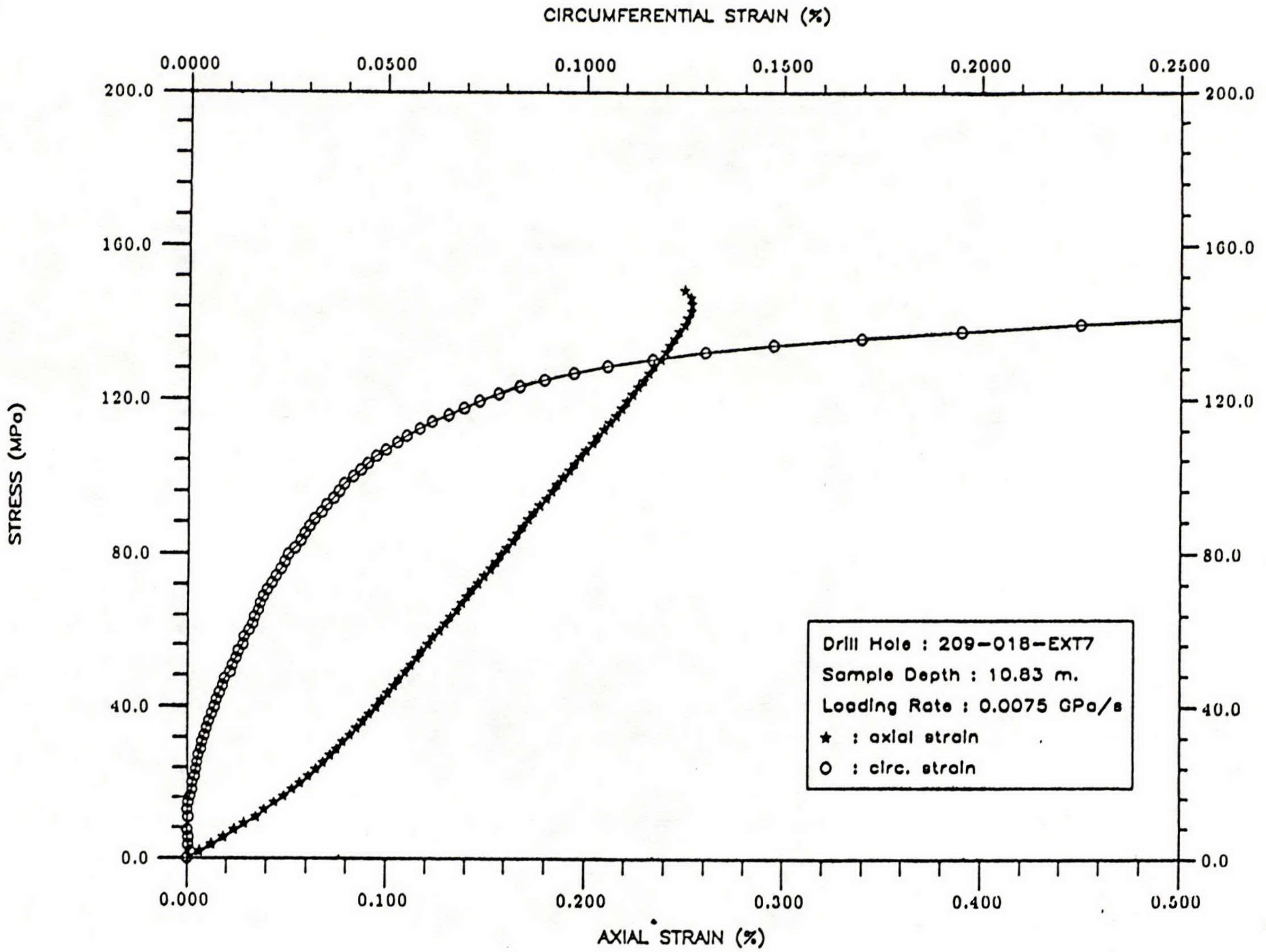

Figure 20 Axial and circumferential stress/strain curves for URL loading rate specimens

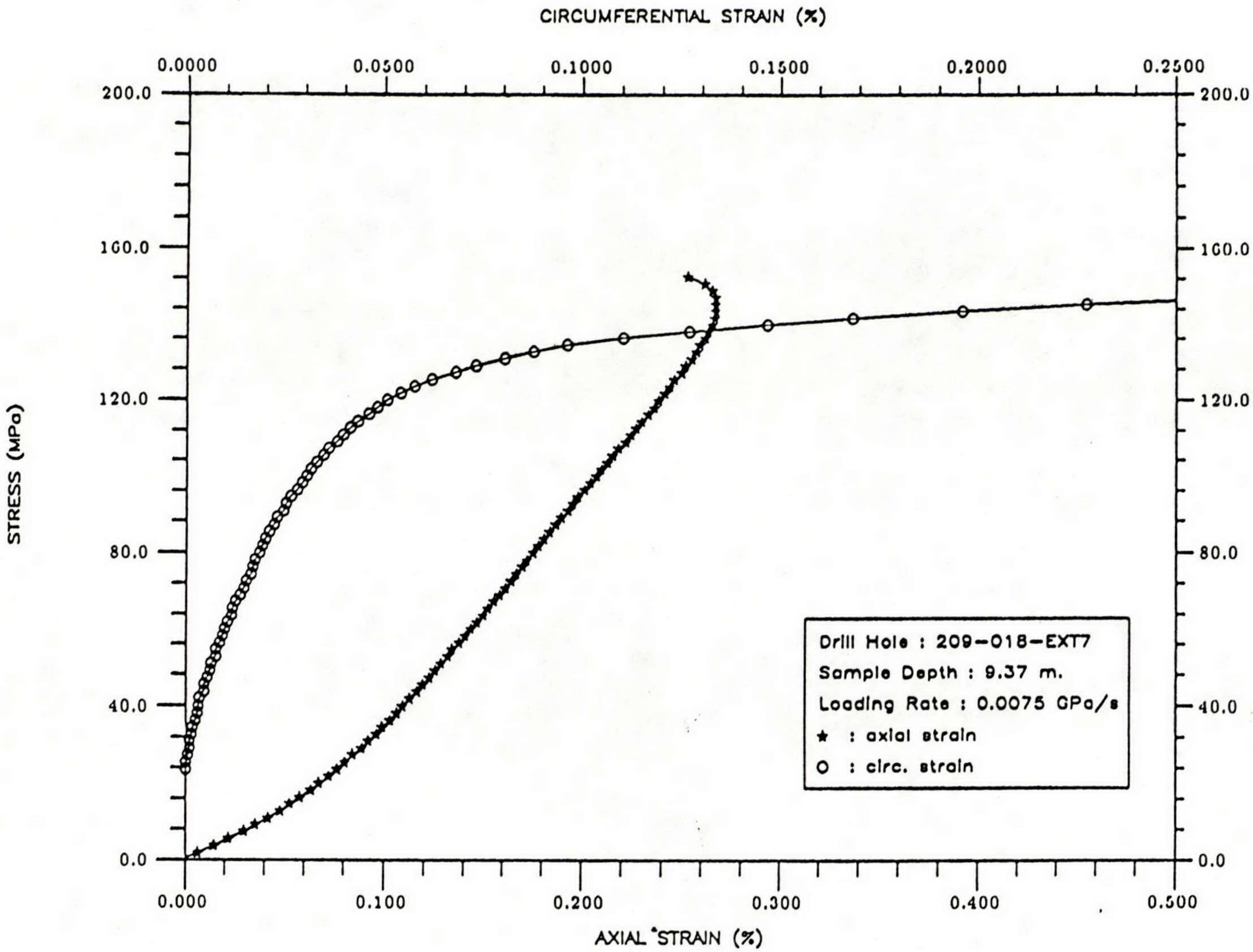

Figure 19 Axial and circumferential stress/strain curves for URL loading rate specimens

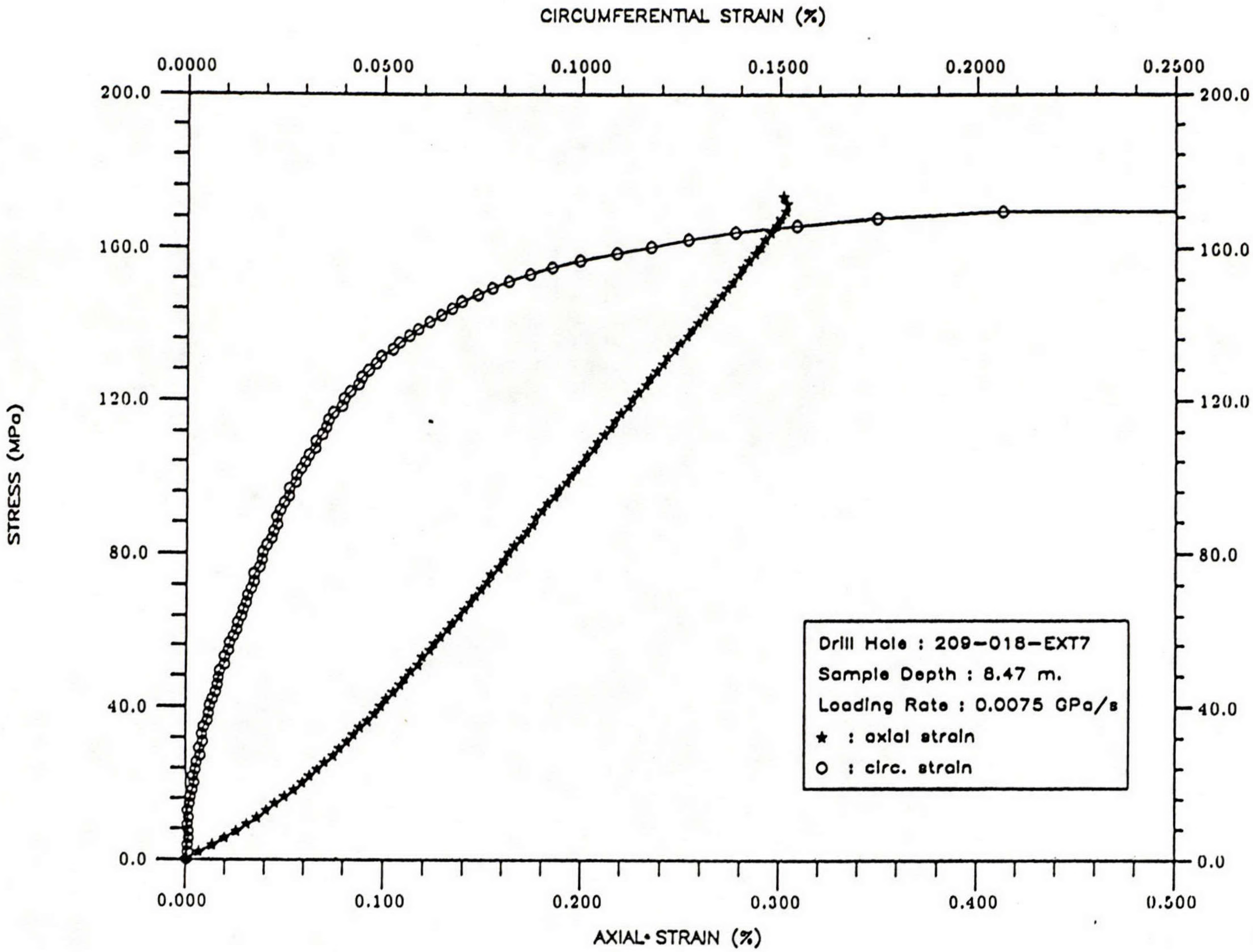

Figure 18 Axial and circumferential stress/strain curves for URL loading rate specimens

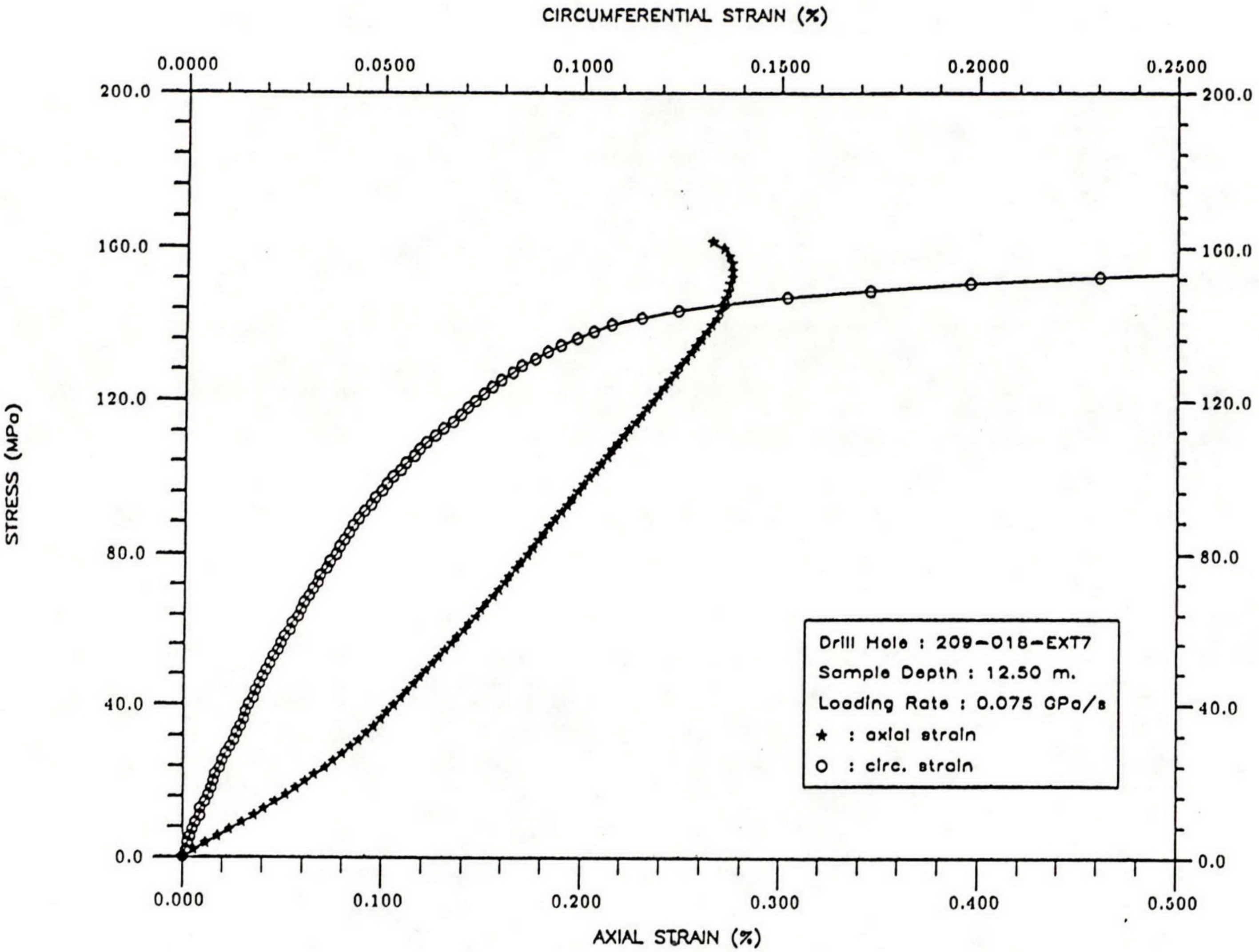

Figure 17 Axial and circumferential stress/strain curves for URL loading rate specimens

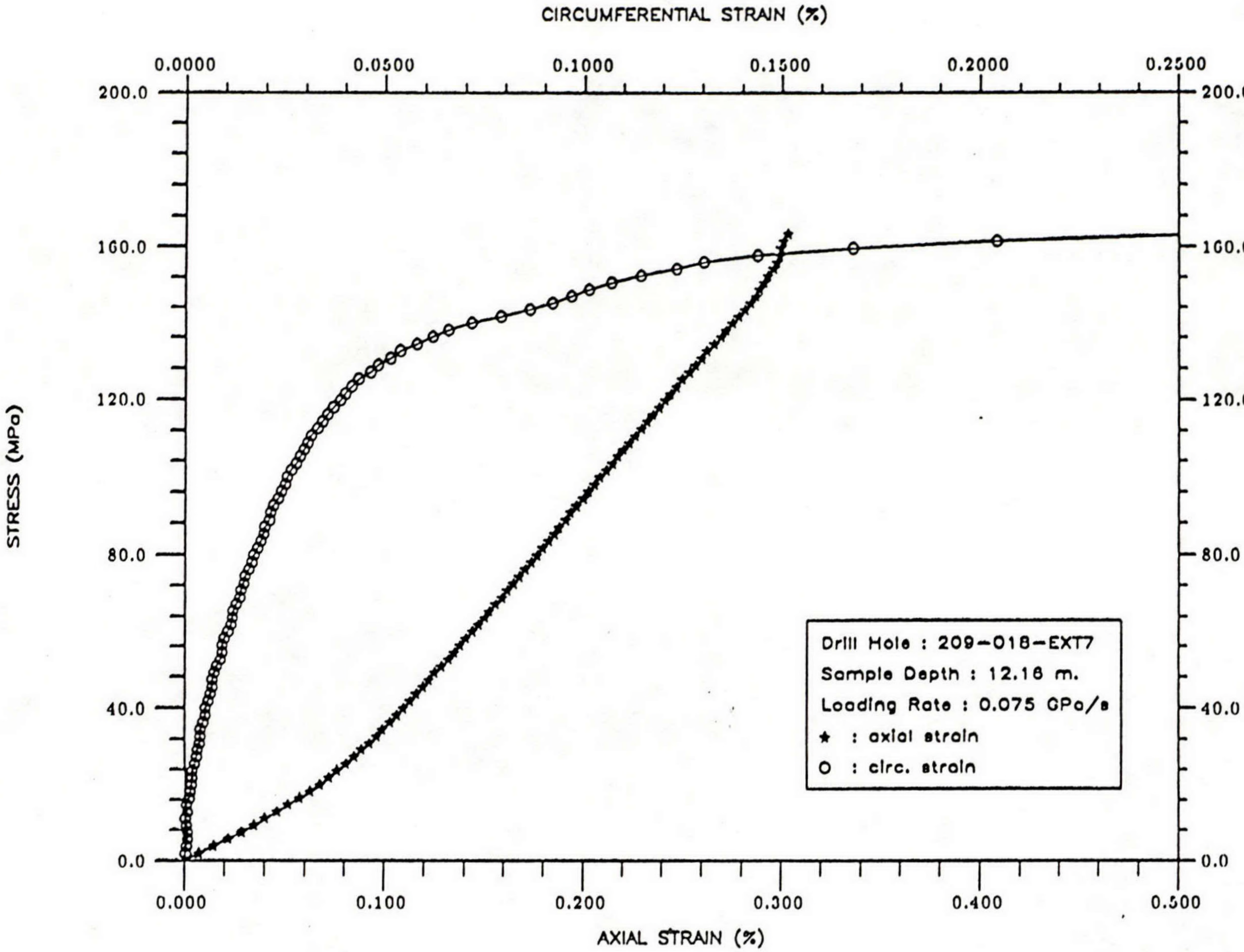

Figure 16 Axial and circumferential stress/strain curves for URL loading rate specimens

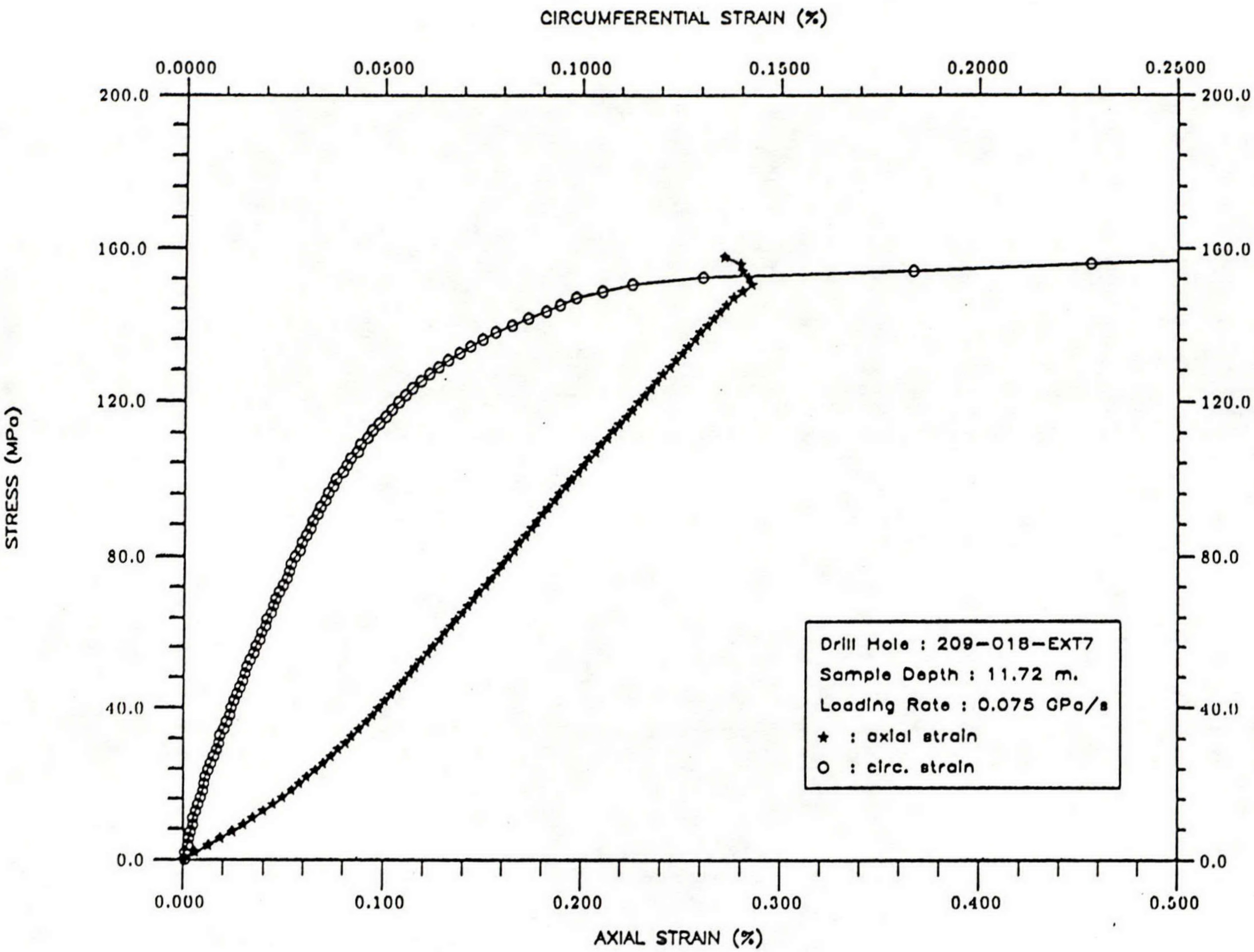

Figure 15 Axial and circumferential stress/strain curves for URL loading rate specimens

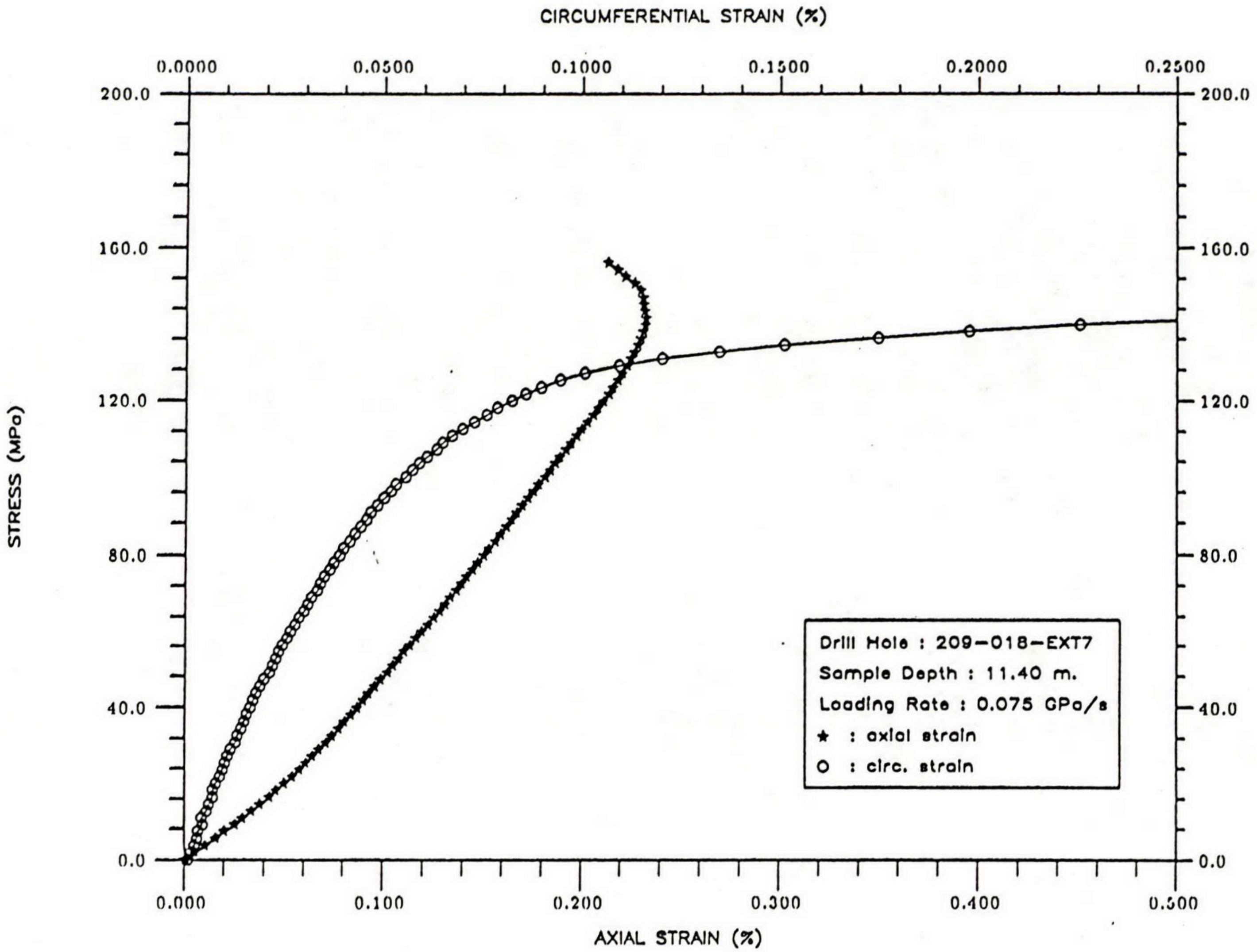

Figure 14 Axial and circumferential stress/strain curves for URL loading rate specimens

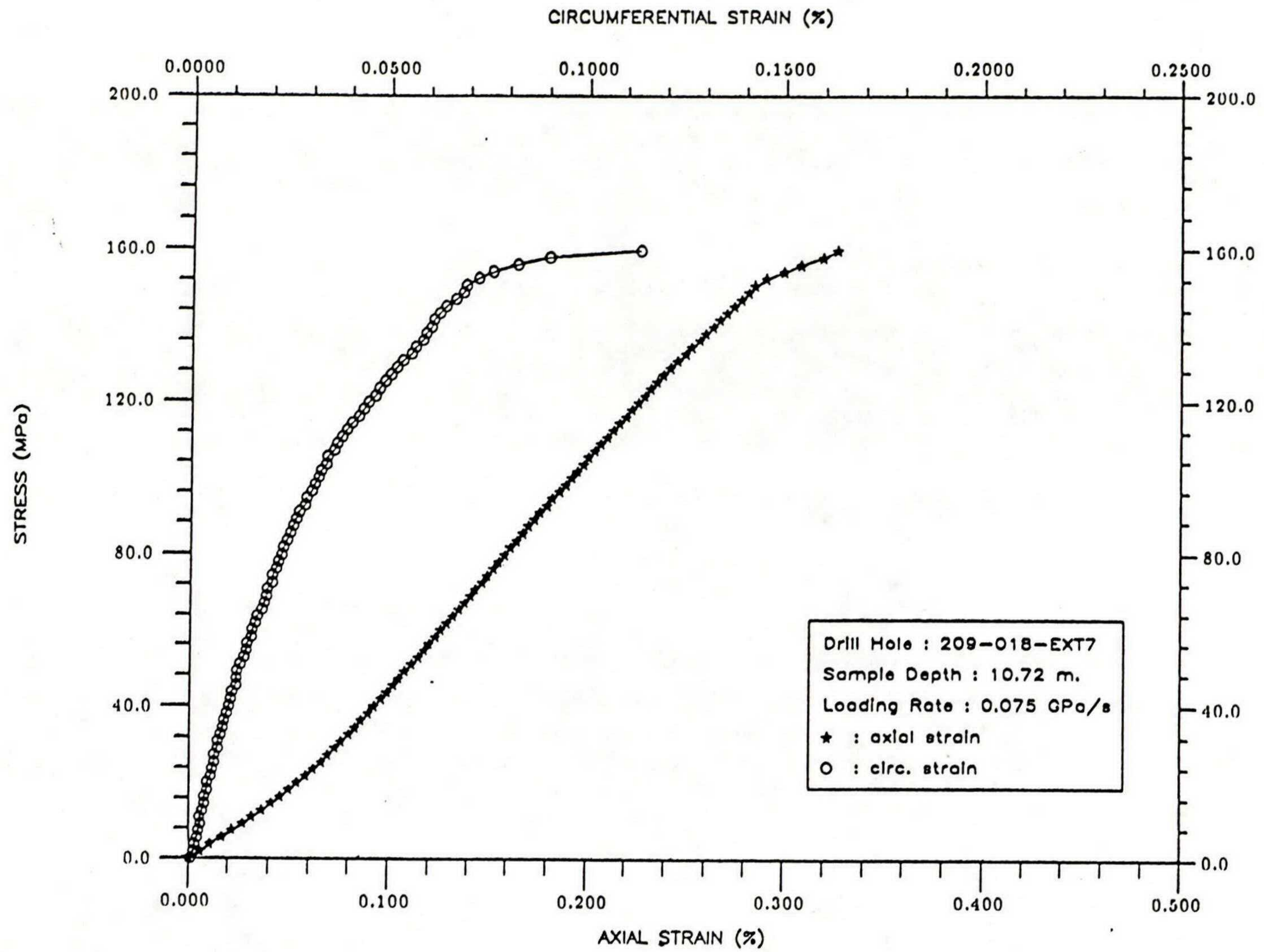

Figure 13 Axial and circumferential stress/strain curves for URL loading rate specimens

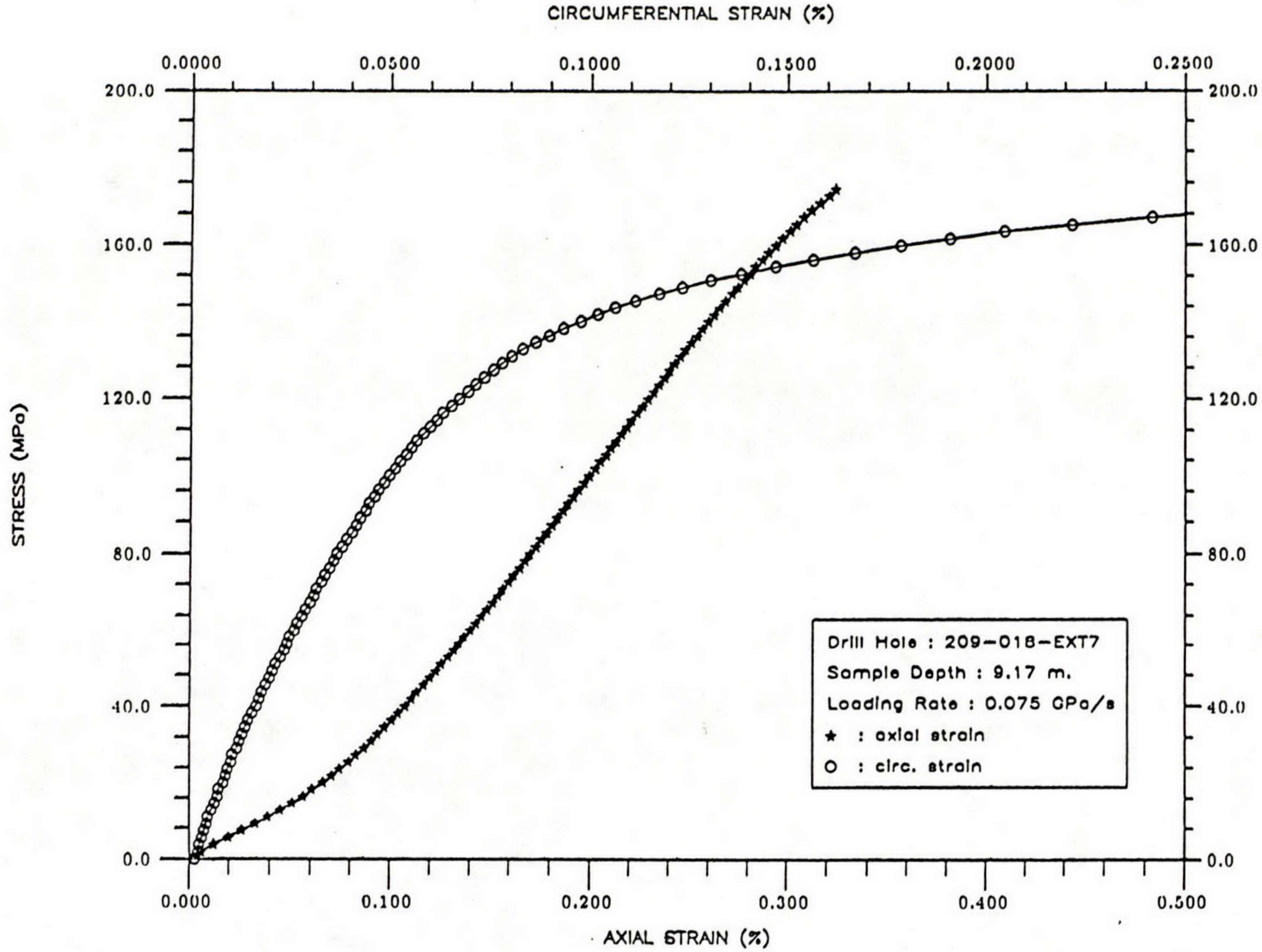

Figure 12 Axial and circumferential stress/strain curves for URL loading rate specimens

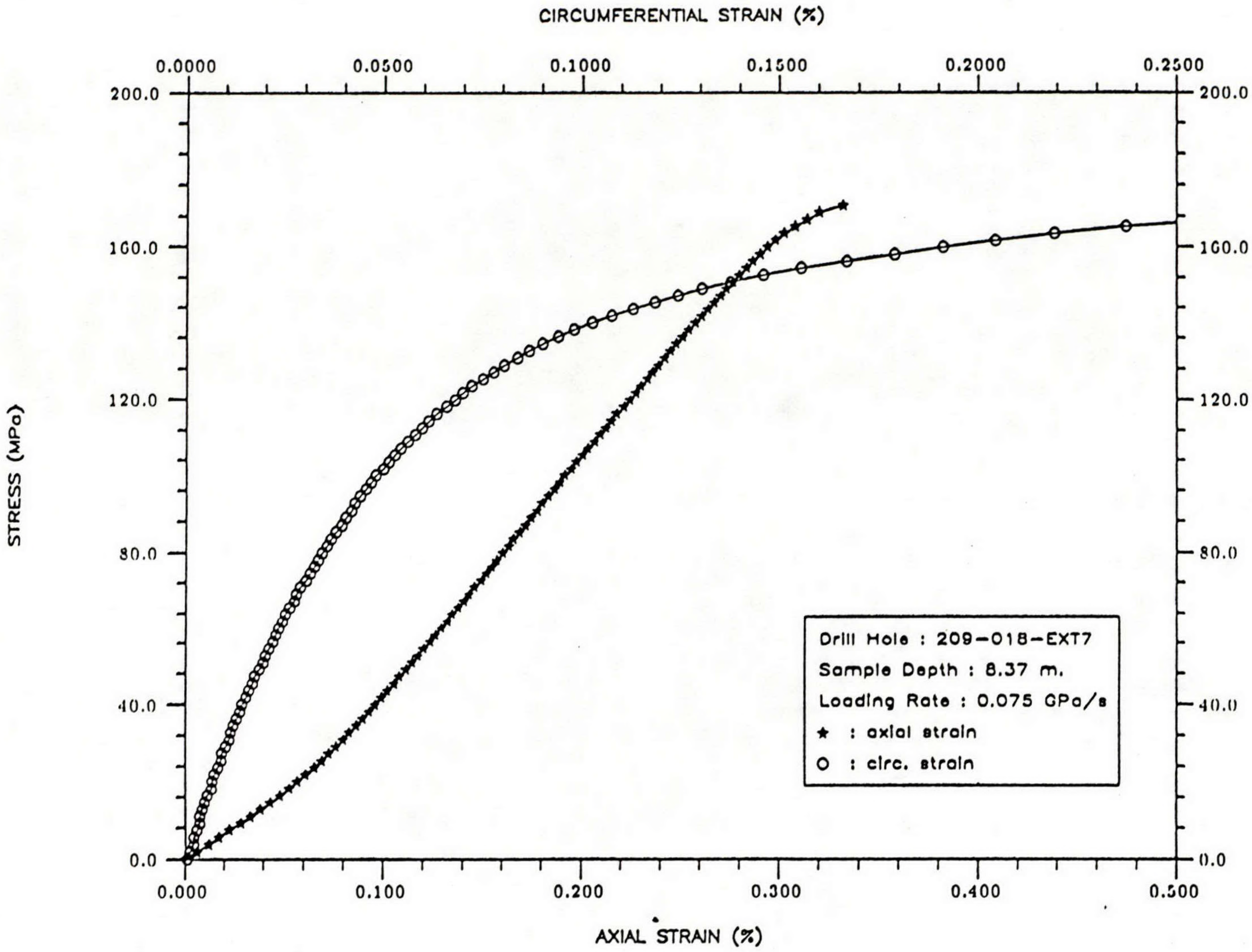

Figure 11 Axial and circumferential stress/strain curves for URL loading rate specimens

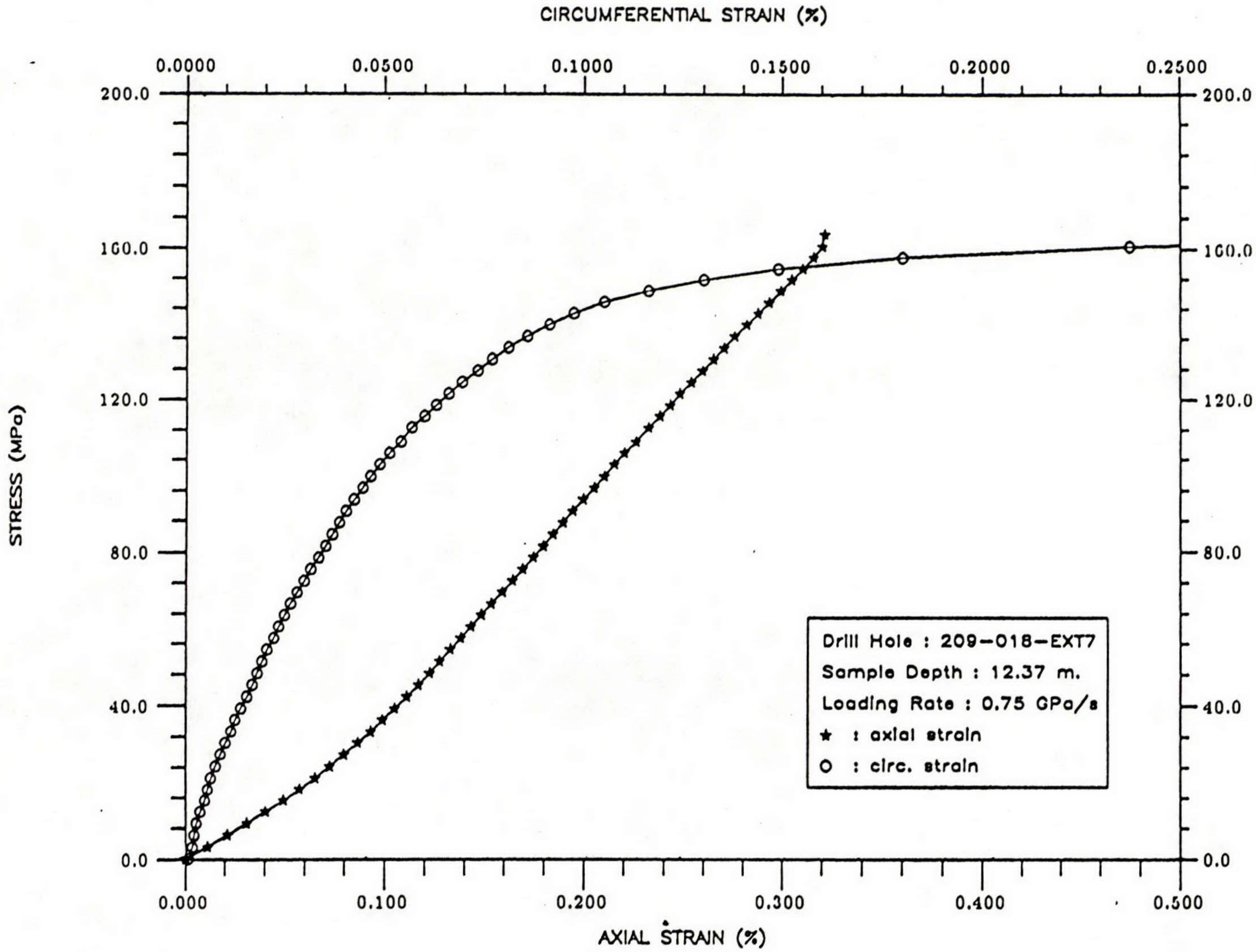

Figure 10 Axial and circumferential stress/strain curves for URL loading rate specimens

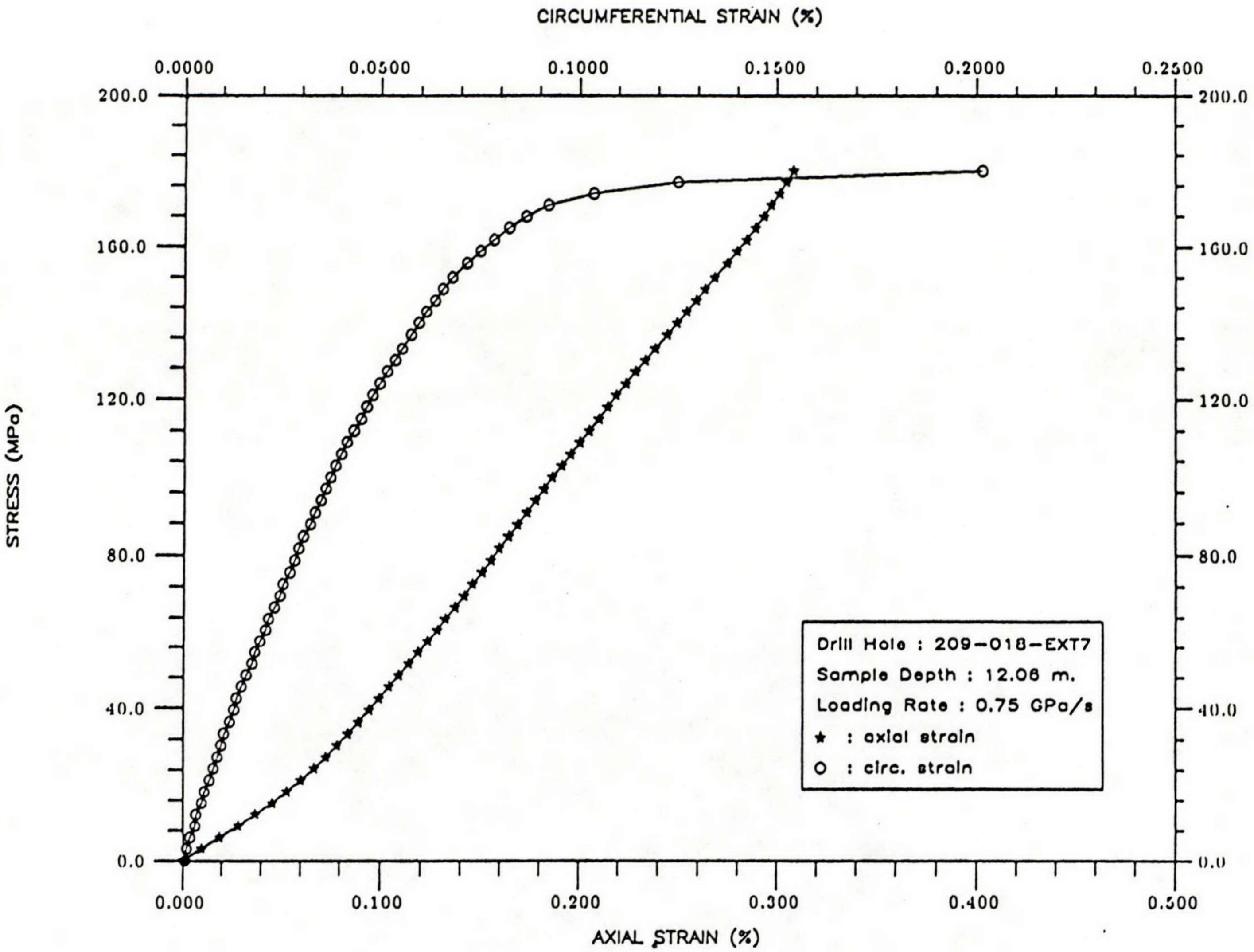

Figure 9 : Axial and circumferential stress/strain curves for URL loading rate specimens

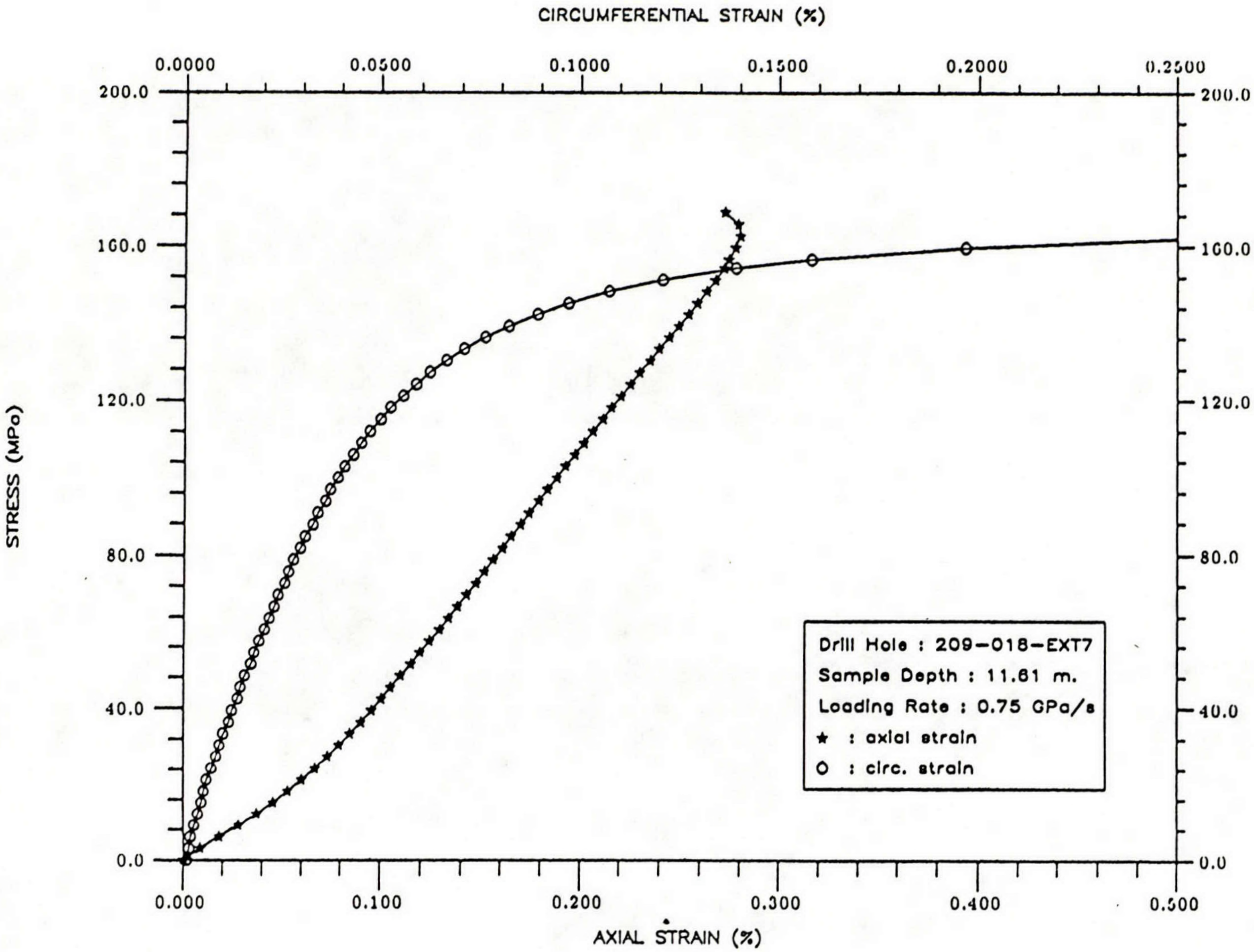

Figure 8 : Axial and circumferential stress/strain curves for URL loading rate specimens

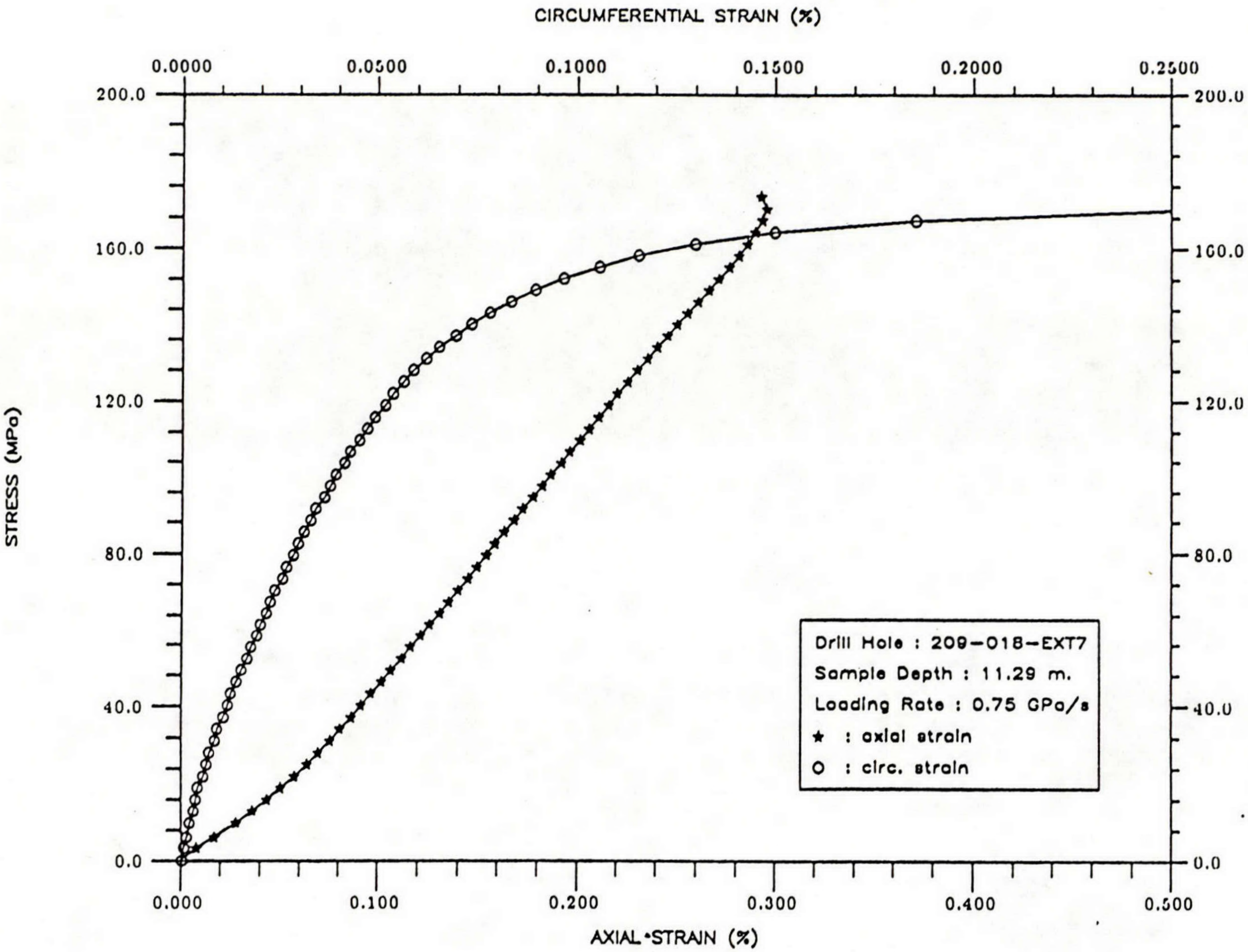

Figure 7 : Axial and circumferential stress/strain curves for URL loading rate specimens

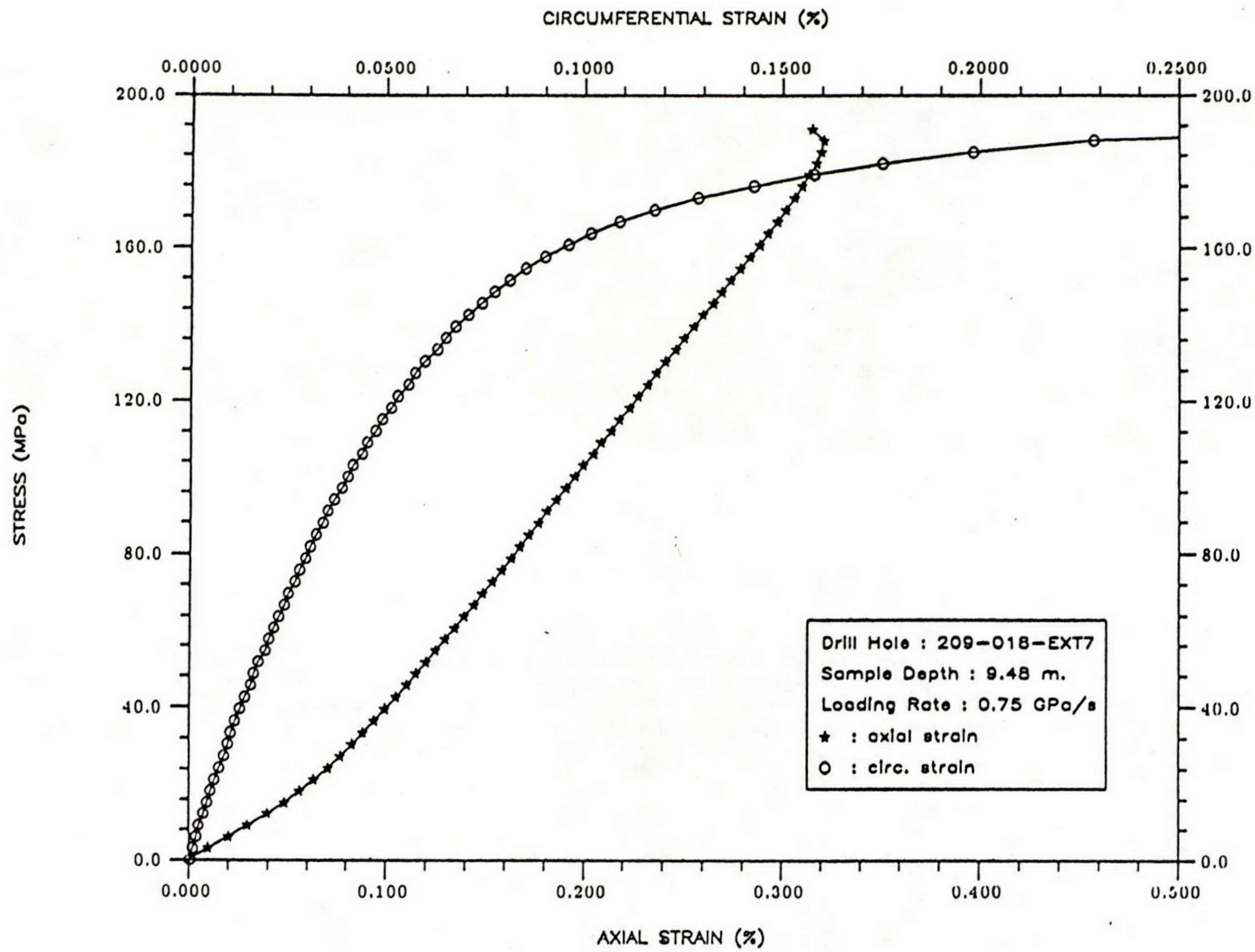

Figure 6 : Axial and circumferential stress/strain curves for URL loading rate specimens

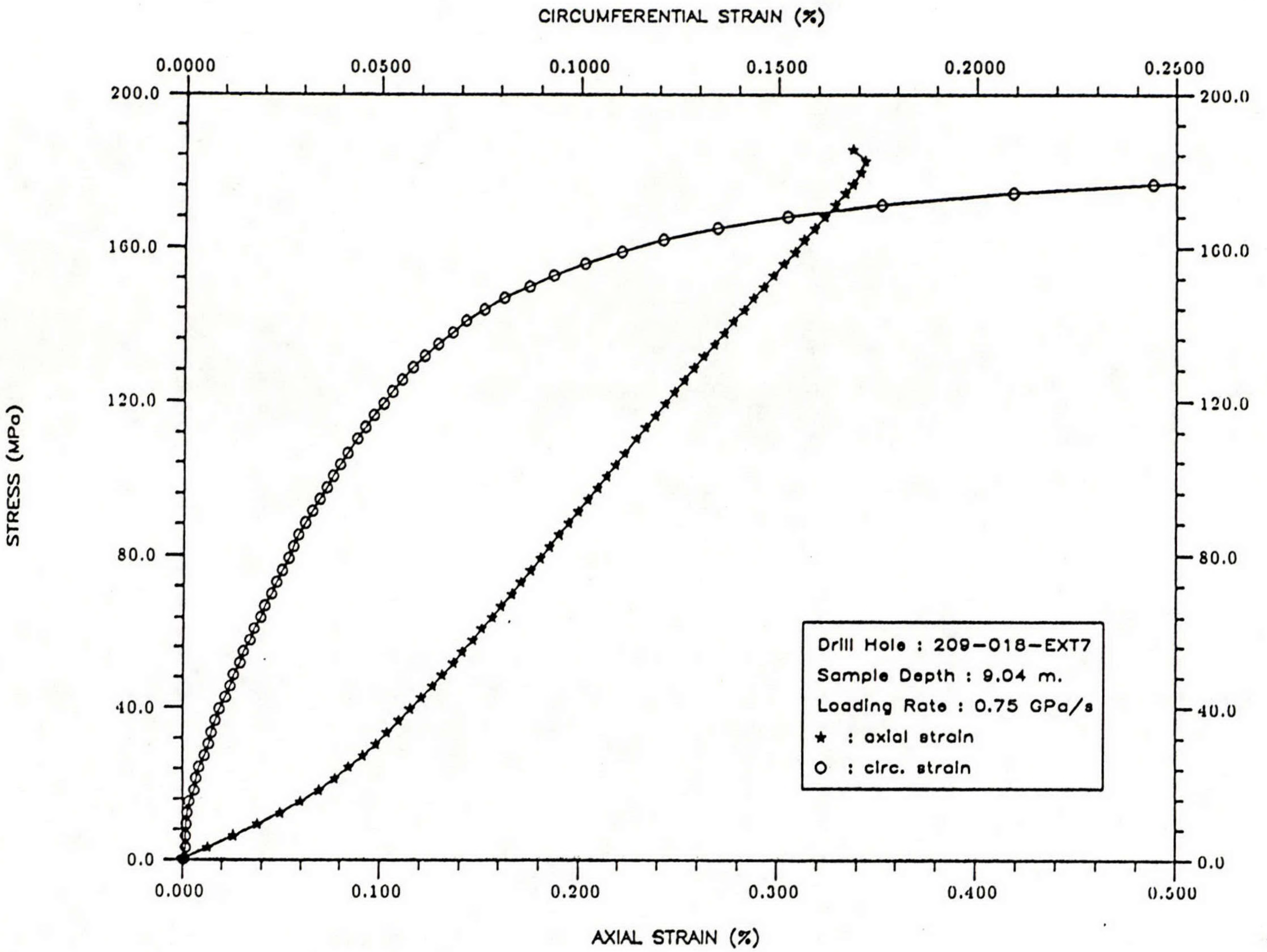

Figure 5 : Axial and circumferential stress/strain curves for URL loading rate specimens

REFERENCES

1. Brace, W.F. An Extension of the Griffith Theory of Fracture to Rocks, Journal of Geophysical Research, Volume 65, no.19, p.p. 3477-3479, 1960.

2. Griffith, A.A. The Theory of Rupture, Proceedings of the 1st International Congress on Applied Mechanics, 1924.

3. Hardy, H.R. Jr. Technical Memorandum 24/59-MIN, 3rd Symposium on Rock Mechanics, 1959.

4. Hunter, G.P. Strain Distrbution of Rock Under Uniaxial Compression, Student work term report, 1989.

5. Jaeger, C. Rock Mechanics and Engineering, Cambridge University Press, p.p. 68-77, 1972.

6. Vutukuri, V.S., Lama, R.D., Saluja, S.S. Handbook on Mechanical Properties of Rocks. Vol. 1, p.p. 44-50, Trans Tech Publications, 1974.

RECOMMENDATIONS

It is recommended that investigations into the feasibility of the long-term storage of nuclear waste in formations such as the Pinawa batholith be encouraged and continued.

Tests that replicate the magnitude of time involved in this type of storage are necessary to fully understand the effects of load on a rock mass over such an extended period. Tests that investigate the relationships between depth and load carrying capability as well as the effects of heat on the strength of the in situ rock are also recommended.

Many other factors may also bear relevance on such storage. Natural geologic occurrences including earthquakes, the movement of the storage area through plate tectonics, and effects of ground water also need to be taken into consideration when the long term storage of potentially dangerous waste is the issue.

CONCLUSIONS

It was concluded that the uniaxial compressive strength of the granitic samples tested was directly affected by loading at different load rates. A decrease in loading rate resulted in a decrease in the uniaxial compressive strength, and sample failure at a lower mean load.

Young's modulus and Poisson's ratio were not affected by reduced loading rates.

It was also concluded that due to the end platens producing uneven regions of stress, no one rock failure theory fully describes the observed failure characteristics, but the cumulation of end platen effects and accepted failure theories can adequately explain observed failure characteristics.